Int J Adv Manuf Technol (2013) 68:651–662
DOI 10.1007/s00170-013-4786-3

ORIGINAL ARTICLE

Relations between the stress components and cross-sectional distortion of thin-walled rectangular waveguide tube in rotary draw bending process

Huawen Shen · Yuli Liu · Haiyan Qi · He Yang · Shuhui Zhou

Received: 23 July 2012 / Accepted: 21 January 2013 / Published online: 2 February 2013

Abstract The significant cross-sectional distortion is one of the major problems in the bending of thin-walled rectangular waveguide tube. The cross-sectional distortion, which contains the flange distortion and the web distortion, depends on the stress components distribution. In this paper, the cross-sectional distortion characteristics are investigated using a three-dimensional finite element (FE) model. Results show that: the maximum flange distortion locates at the symmetric line; meanwhile, the maximum web distortion locates at the extrados ridge of the tube. The deformation zone of the tube can be divided into three sub-zones considering the loads and deformation, viz., the clamp die affect zone, the middle zone, and the mandrel/cores affect zone. Then the underlying relations between the cross-sectional distortion and the stress components are obtained. It is found that the flange distortion has a close relation with the circumferential stress. At the same time, the web distortion is relevant to both the tangential and the circumferential stress. The above relations are verified by FE models with different cores number. Moreover, some guidelines are introduced to help reduce the cross-sectional distortion.

Keywords Cross-sectional distortion · Rectangular waveguides · Aluminum alloys · Rotary draw bending · Simulation

H. Shen · Y. Liu (✉) · H. Qi · H. Yang · S. Zhou
State Key Laboratory of Solidification Processing,
School of Materials Science and Engineering,
Northwestern Polytechnical University, Xi'an 710072, China
e-mail: lyl@nwpu.edu.cn

1 Introduction

Due to the high strength/weight ratio, good vibration absorbability, and low waveguide loss, the aluminum alloys thin-walled rectangular waveguide tube (TWRWT) components are widely used in aviation, aerospace, and automobile. The rotary draw bending (RDB) process is one of the most commonly used methods in the bending of TWRWT [1]. Compared with other processes, such as stretch bending, rolling bending, and compression bending, the RDB process has characteristics of quick batch production capability, high efficiency, cost saving, and stable quality [2, 3]. However, the complex contact conditions of the TWRWT with multiple dies can easily induce defects or instabilities, such as wrinkling, over thinning, and cross-sectional distortion. Especially, the cross-sectional distortion, which contains not only the concave of the flange but also the convex of the web, directly weakens the mechanical behaviors and the ability of signal wave transmission. The cross-sectional distortion depends on the stress components distribution [4]. Therefore, in order to control the cross-sectional distortion efficiently, it is crucial to understand the relation between the stress components and the cross-sectional distortion.

Over the years, many studies have been conducted on the cross-sectional distortion of tube bending through analytic, experimental, or numerical methods. Unfortunately, most of them focused on circular tube bending [5–9]. As for rectangular tube bending, most researches concentrated on predicting the cross-sectional deformation of rectangular tube in stretch bending process through analytic methods. Miller [10] assumed that the loads and deformation were uniform along the length and presented a formulation to estimate the

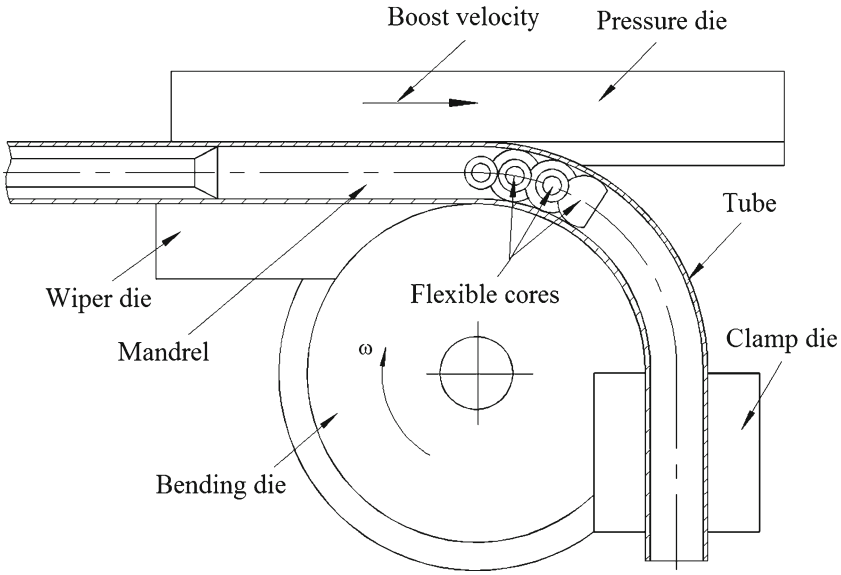

Fig. 1 Schematic diagram of TWRWT in RDB process

deformation of the rectangular cross-sectional. Based on the deformation theory of plasticity along with the energy method using appropriate shape function, Paulsen [4, 11] provided explicit solutions of cross-sectional deformation of rectangular hollow section in stretch bending. Welo [12, 13] established an analytical moment curvature model which was used to predict cross-sectional distortion of rectangular profiles in stretch bending. However, the loads and deformation of the tube are not uniform along the length in RDB process [14]. Thus, analytic methods are difficult to express the cross-sectional distortion of TWRWT in RDB process due to the sophisticated stress distribution. In experimental studies, Liu [15] carried out experiments with different process parameters to predict and control the cross-sectional distortion. Though the experimental methods can provide relatively credible results, the obtained data are only suitable for the bending with the same forming conditions. Finite element (FE) methods have been proven to be a well-suited tool for design and product optimization in tube bending [16–19]. Recently, many scholars have tried to control the cross-sectional distortion by changing the process parameters [20, 21], but researches aiming at the characteristics and mechanism of the cross-sectional distortion of TWRWT in RDB process are still scant.

The above findings and results are helpful for a better understanding of tube bending process. However, with lack of understanding, the characteristics and mechanism of the cross-sectional distortion, in practice, the feasible bending parameters are still obtained through the empirical data or operator-based "error and trial" method. Thus, the characteristics of TWRWT in RDB process are identified in this paper. Then, the tube is divided into three sub-zones considering the loads and deformation. In addition, the underlying relations between the cross-sectional distortion and the stress components in each sub-zone are investigated to reveal the mechanism of the cross-section distortion.

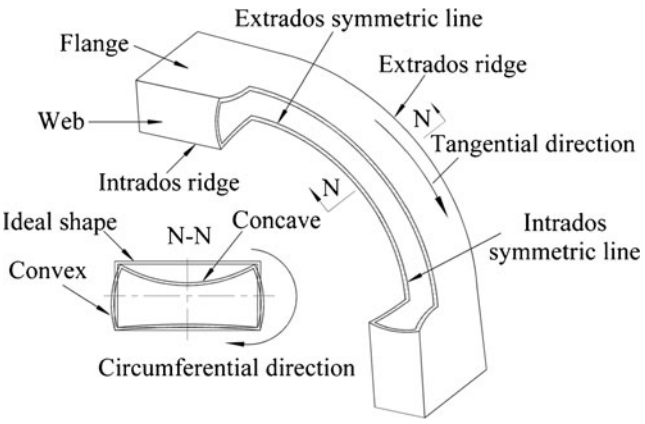

Fig. 2 The cross-sectional distortion of TWRWT bent

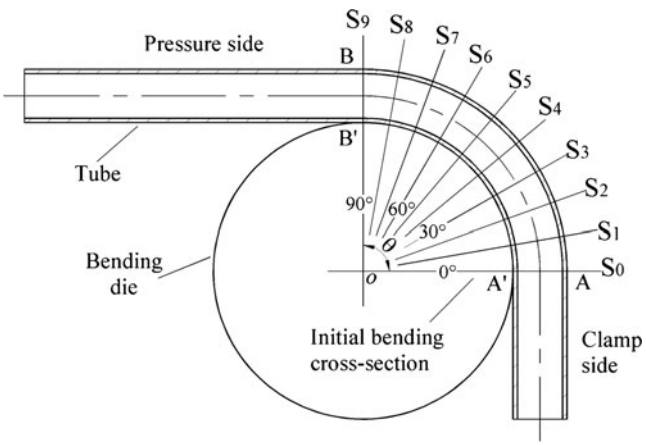

Fig. 3 The typical sections in the bent zone

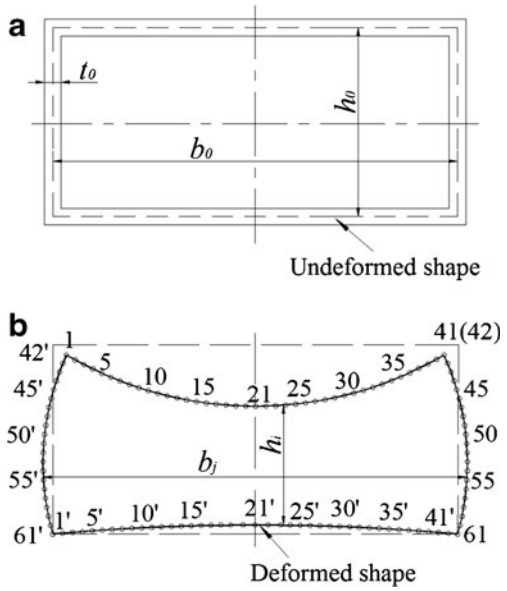

Fig. 4 Geometric parameters of the cross-section: **a** undeformed and **b** deformed

2 Description of the cross-sectional distortion of TWRWT in RDB process

2.1 Steps of RDB process

Figure 1 shows the schematic diagram of TWRWT in RDB process. The RDB process comprises three steps: in step 1, the tube is fixed at one end while the other end is guided by the pressure die; then the mandrel and the flexible cores are placed in position. In step 2, as the bending die and the clamp die rotate as well as the boosting of the pressure die, the tube is bent continuously. In step 3, the mandrel and the flexible cores are retracted. During the bending process, concave appears in the flanges while convex appears in the webs (Fig. 2).

2.2 Description of the cross-sectional distortion of TWRWT

The tube bent with a 90° bending angle (θ in Fig. 3) is taken as the main research object. In order to investigate the distribution of cross-sectional distortion of the TWRWT, ten typical sections with the angle interval of 10° are selected in the bent zone from the initial bending cross-section (Fig. 3(A–A')).

As shown in Fig. 4a, the geometric parameters of the cross section of rectangular tube are normalized by the mid-surface height (h_0), width (b_0), and thickness (t_0), respectively. The tube used in this study is measured as 23.86× 11.2×1 mm. The flange distortion in each typical section are marked as δ_{h_i} (i=1, 2, 3 … 41), $\delta_{h_{\max}}$ is the maximum δ_{h_i}. δ_{b_j} (j=42, 43, 44 … 61) are the distortion of the web in each typical section and $\delta_{b_{\max}}$ is the maximum δ_{b_j}. The values of δ_{h_i} and $\delta_{\mathrm{b_j}}$ are expressed as formulas (1) and (2), respectively.

$$\delta_{h_i} = \frac{|h_0 - h_i|}{h_0} \times 100\% \tag{1}$$

$$\delta_{b_j} = \frac{|b_0 - b_j|}{b_0} \times 100\% \tag{2}$$

Where h_i (i=1, 2, 3 … 41) are the distances between nodes i and i' after deformation; b_j (j=42, 43, 44 … 61) are the deformed distances between nodes j and j' after deformation (Fig. 4b).

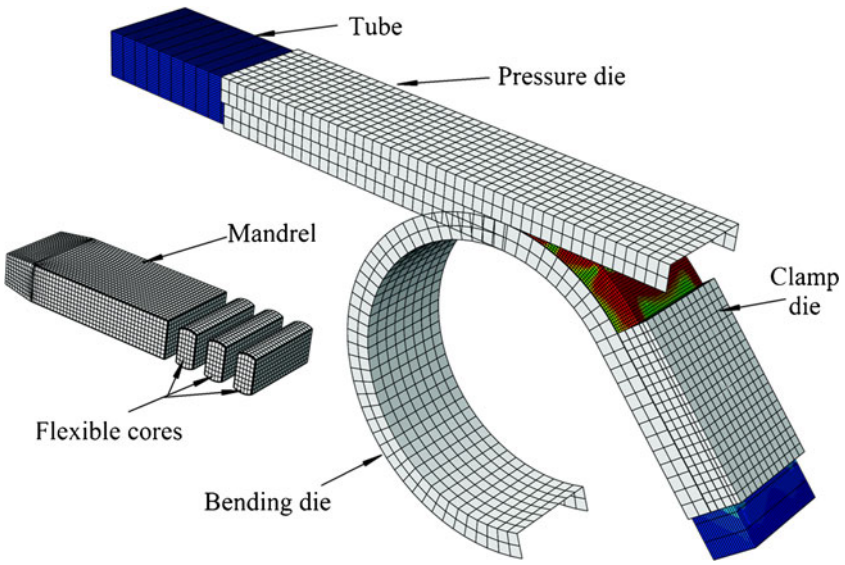

Fig. 5 Diagram of the FE model for the TWRWT in RDB process

Table 1 Mechanical properties of 3A21 rectangular tube

Parameter	Value
Ultimate tension strength σ_b/MPa	151.68
Poisson's ratio γ	0.33
Initial yield stress $\sigma_{0.2}$/MPa	99.7
Strength coefficient K/MPa	225.28
Material constant b	0.0016
Hardening exponent n	0.145
Young's modulus E/GPa	60.2
Density ρ/kgm^{-3}	2,730

3 Establishment of the 3D-FE model for TWRWT in RDB process

3.1 Key techniques of the 3D-FE model

As shown in Fig. 5, a three-dimensional (3D) elastic-plastic FE model is established based on the ABAQUS/explicit platform. The tube material used in this paper is a 3A21 aluminum alloy rectangular tube. Its hardening behavior is described by:

$$\sigma = K(\varepsilon + b)^n \tag{3}$$

Uniaxial tension test is used to obtain the material properties (Table 1). Joints between mandrel and cores are simplified as hinge connection. Friction between tube and dies is modeled with classical Coulomb's friction model. Table 2 shows the friction coefficients on multiple contact interfaces [22]. In the modeling, four-node shell elements with reduced integration are used to model the tube. The 3D four-node rigid elements are used for dies.

3.2 Evaluation of the 3D-FE model

To examine the reliability of the model, the experiment for bending of 3A21 aluminum alloy TWRWT is carried out using a W27YPC-63 microcomputer-controlled bender. The forming parameters used in experiment and FE simulation are shown in Table 3.

Figure 6 shows the TWRWT bent part obtained by experiment and simulation. As shown in Fig. 7, the simulated results of $\delta_{h_{\max}}$ and $\delta_{b_{\max}}$ agree well with the experimental ones and the maximum relative error between them is less than 10 %. The discrepancy is mainly caused by the idealized conditions used in the FE simulation, such as constant friction coefficients, etc. In view of this, the results obtained by the FE model are reliable.

4 Results and discussion

4.1 Distribution characteristics of the cross-sectional distortion of TWRWT

4.1.1 Distribution characteristics of δ_{h_i}

Figure 8 shows the distribution of flange distortion δ_{h_i} in typical sections S_0, S_1, S_2 … S_9. It can be found that the distribution of δ_{h_i} is bilateral symmetry. In addition, its axis of symmetry is line 21–21′ in each section. The maximum flange distortion $\delta_{h_{\max}}$ occurs at the symmetric line in each section. Moreover, section S_1 has the ultimate flange distortion value in the whole bent zone.

It can also be found that the middle bent zone S_1–S_5 has larger distortion than the initial bent cross-section S_0 and the end bent zone S_6–S_9. That is because during the bending step, the initial bent zone is constrained by the clamp die; meanwhile, the end bent zone is supported by the mandrel and cores. However, both the restriction effect and the internal support are useless to the middle bent zone.

Considering this, the deformation zone of TWRWT can be divided into three sub-zones, viz., the clamp die affect zone (CAZ), the middle zone (MZ), and the mandrel/cores affect zone (MCAZ) (Fig. 9).

Table 2 Friction conditions on multiple contact interfaces

Contact interfaces	Friction coefficient
Tube-clamp die	0.6
Tube-bending die	0.3
Tube-pressure die	0.3
Tube-wiper die	0.14
Tube-mandrel	0.1
Tube-cores	0.06

Table 3 Forming parameters used in experiment and FE simulation

Parameter	Value
Bending radius R_d (mm)	40
Bending velocity ω (rad/s)	0.5
Boost velocity V_p (mm/s)	23.5
Mandrel retracting velocity V_m (mm/s)	0.14
Clearances between mandrel die/tube (mm)	0.1
Clearances between other dies/tube (mm)	0

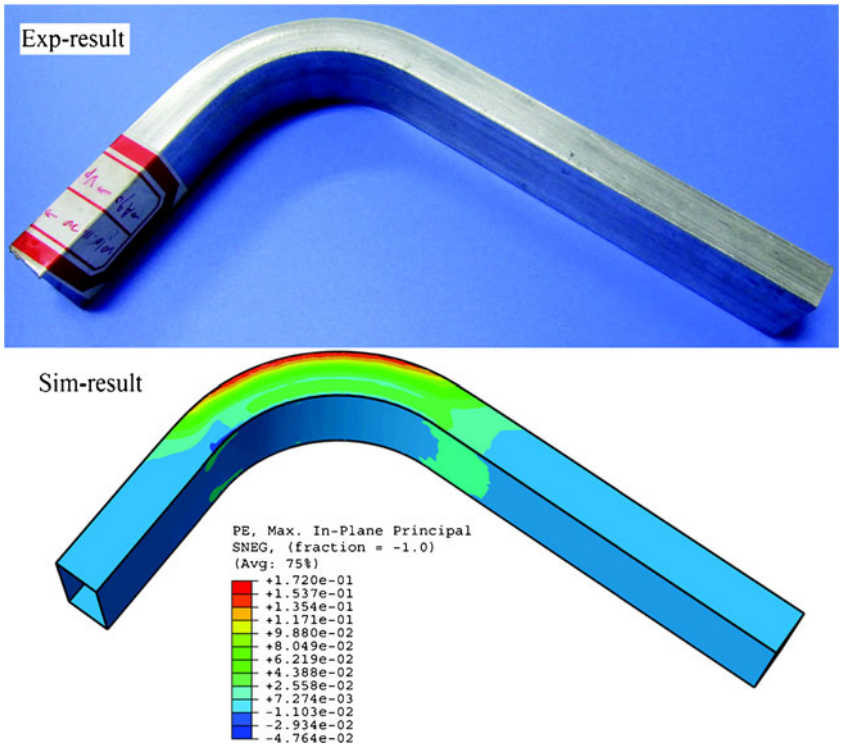

Fig. 6 The experimental and simulated TWRWT bent

4.1.2 Distribution characteristics of δ_{b_j}

Figure 10 shows the distribution of δ_{b_j} in typical sections S_0, S_1, S_2 … S_9. It is obvious that the maximum distortion of web $\delta_{b_{\max}}$ occurs at the extrados ridge of the tube, viz., nodes 42–42′ in each section. Besides, δ_{b_j} in the CAZ are very small due to the restriction effect of the clamp die. However, the convex of web enlarges the clearances between the web and mandrel/cores, the internal support effects of mandrel/-cores to the web are small. As a result, δ_{b_j} in the MCAZ S_6–S_9 are as large as those in the MZ S_1–S_5. It can also be found that the distortion of web δ_{b_j} are smaller than the distortion of flange δ_{h_i}, that is why the former ones are usually neglected [14, 15]. However, sometimes, for example in the absence of flexible cores, δ_{b_j} are too large to be neglected (Fig. 11).

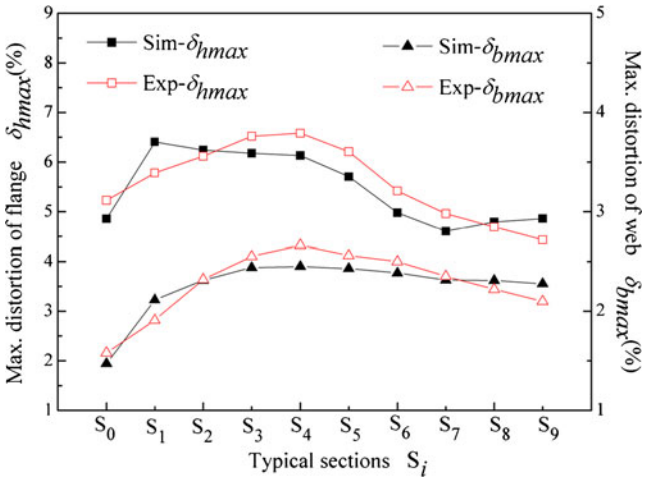

Fig. 7 The experimental and simulated results of cross-sectional distortion

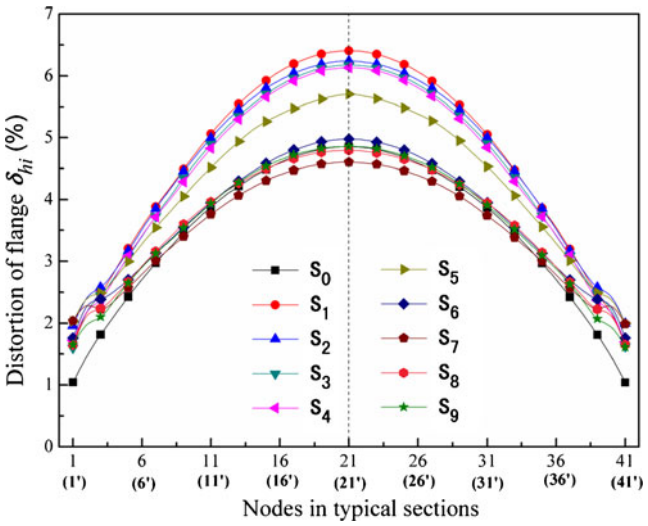

Fig. 8 The flange distortion in different typical sections

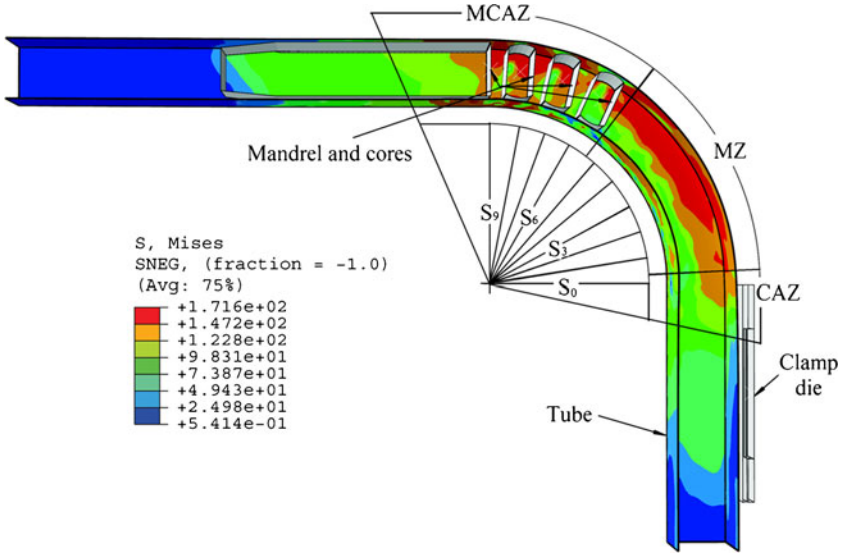

Fig. 9 Diagram of division of the TWRWT (three cores)

4.2 Relation between the cross-sectional distortion and the stress components

4.2.1 Relation between $\delta_{h_{\max}}$ and the circumferential stress σ_β

Figure 12 shows the maximum flange distortion $\delta_{h_{\max}}$ and the circumferential stress σ_β at the extrados symmetric line (Fig. 2) in different typical sections during the bending stage. Clearly, some fluctuation of σ_β appear in the MCAZ. Furthermore, the MCAZ is moved backwards continuously, that is because the tube is boosted forwards while the mandrel is fixed in the bending step. Moreover, the area size of the MCAZ enlarges at first and keeps unchanged after the bending angle 60° (Fig. 12f–i).

It can also be found that $\delta_{h_{\max}}$ keeps increasing both in value and range at first. However, the peak value of $\delta_{h_{\max}}$ seems not to increase but the range still keeps increasing after the bending angle 60° (Fig. 12f–i). When the bending angle reaches 90° (Fig. 12i), $\delta_{h_{\max}}$ reaches the peak value in the MZ. In the subsequent mandrel retracting step, $\delta_{h_{\max}}$ in the original MCAZ increases (Fig. 12j). That is because the internal support effect does no longer exist after the retracting step. Thanks to the harmony of deformation, the distribution of $\delta_{h_{\max}}$ tends to be homogeneous finally.

It is obvious that when the fluctuation in the MCAZ is neglected at first, the general evolvement of the circumferential stress σ_β and the maximum distortion of flange $\delta_{h_{\max}}$ are almost the same. After the bending angle 60°, the distribution of $\delta_{h_{\max}}$ is really identical with the distribution of σ_β in the whole bent zone. That's because the area of MCAZ as well as the peak value of maximum flange distortion is no longer changing after bending angle 60° (see Fig. 12g–i). In other words, the bending process is stable

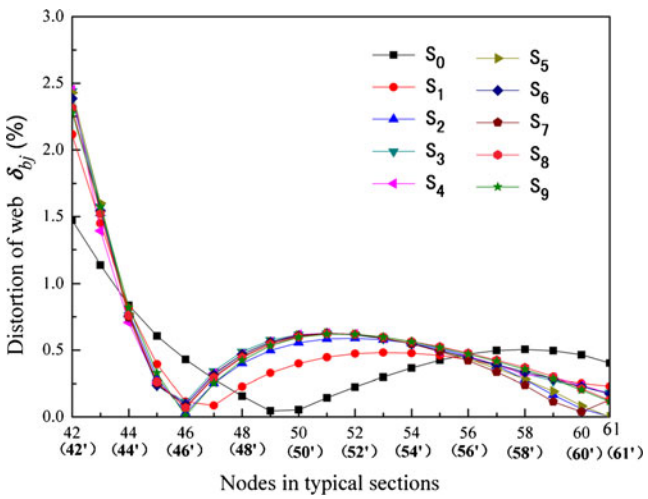

Fig. 10 The web distortion in different typical sections

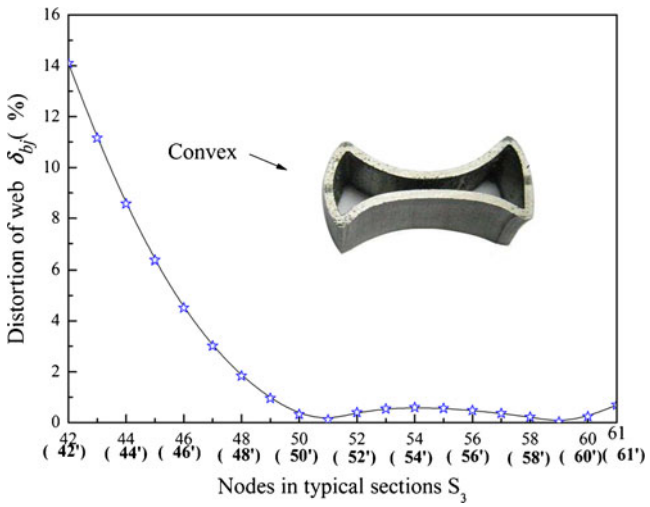

Fig. 11 The distribution of web distortion in the absence of cores

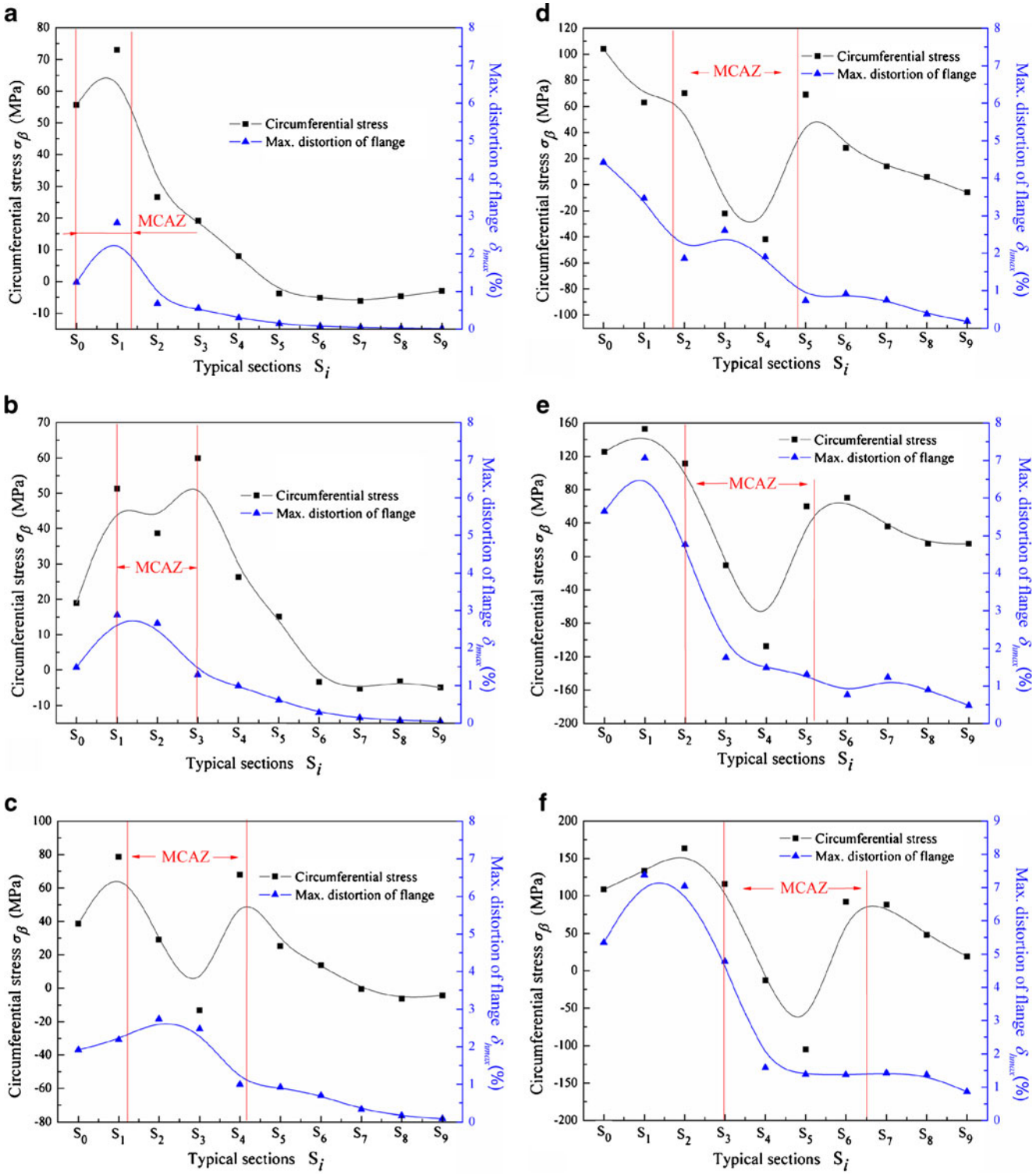

Fig. 12 The circumferential stress and the maximum flange distortion during the bending stage: **a** bending angle, 10°; **b** bending angle, 20°; **c** bending angle, 30°; **d** bending angle, 40°; **e** bending angle, 50°; **f** bending angle, 60°; **g** bending angle, 70°; **h** bending angle, 80°; **i** bending angle, 90°; and **j** after mandrel retracting

since then. Therefore, the whole bent zone follows the identical law between the flange distortion and the circumferential stress.

In summary, it comes to a conclusion that the flange distortion has a close relation with σ_β. The distribution and value of $\delta_{h_{\max}}$ are determined by σ_β.

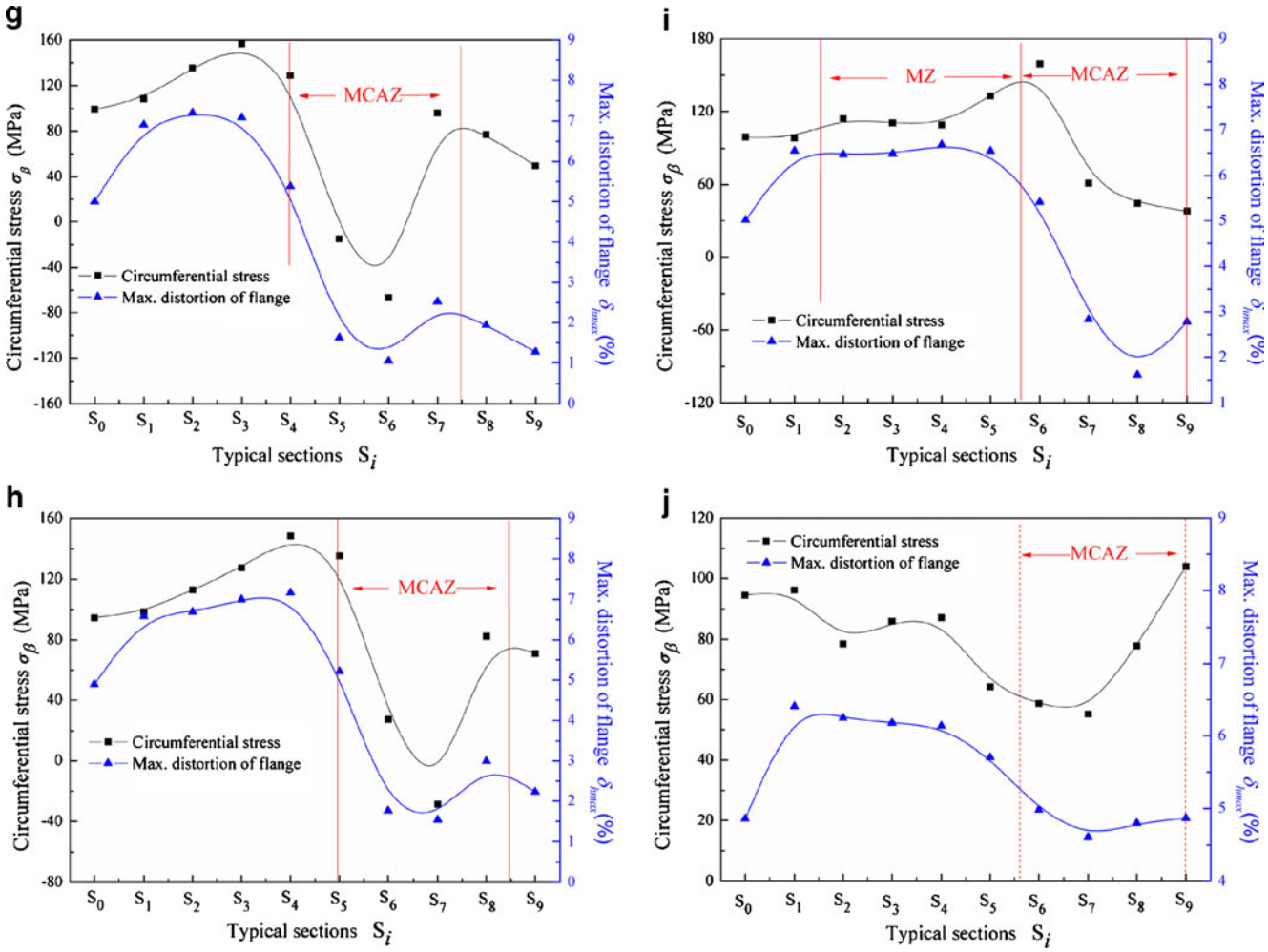

Fig. 12 (continued)

4.2.2 Relation between $\delta_{b_{\max}}$ and the composite stress σ_1

In addition, similar relation can be found when compare the maximum web distortion $\delta_{b_{\max}}$ and the composite stress σ_1 (defined by formula (4)).

$$\sigma_1 = \sqrt{(\sigma_\alpha)^2 + (\sigma_\beta)^2} \tag{4}$$

Where σ_α and σ_β represent the tangential and the circumferential stress, respectively. Figure 13 shows $\delta_{b_{\max}}$ and σ_1 at the extrados ridge (Fig. 2) in different typical sections of the tube during the bending stage, respectively. It can be found that there is relatively small fluctuation of σ_1 in the MCAZ.

Similar to $\delta_{h_{\max}}$, $\delta_{b_{\max}}$ keeps increasing both in the value and range at first. After the bending angle 60°, the peak value of $\delta_{b_{\max}}$ is almost constant (approximately fixed at 2.5 %, shown in Fig. 13f–i). When the bending angle reaches 90°, $\delta_{b_{\max}}$ reaches the peak value both in the MZ and the MCAZ (Fig. 13i). Moreover, the distribution of $\delta_{b_{\max}}$ is homogeneous in general. In the subsequent retracting step, $\delta_{b_{\max}}$ is nearly unchanged (Fig. 13j). That is because the convex of web enlarges the clearances between the web and mandrel/cores, thus the effects of mandrel/cores to the web are smaller than those to the flange.

Clearly, the transformation tendency of $\delta_{b_{\max}}$ and σ_1 are almost the same except for relatively small fluctuation of σ_1 in the MCAZ. The above analysis concludes that the web distortion has a close relation with both σ_α and σ_β. The distribution and value of $\delta_{b_{\max}}$ are determined by a comprehensive effect of the two stress components.

4.3 Verification of the relations via FE models with different cores number

The mandrel die, which comprises a mandrel and several flexible cores, is an important part in RDB process. The internal support provided by the mandrel die has a great

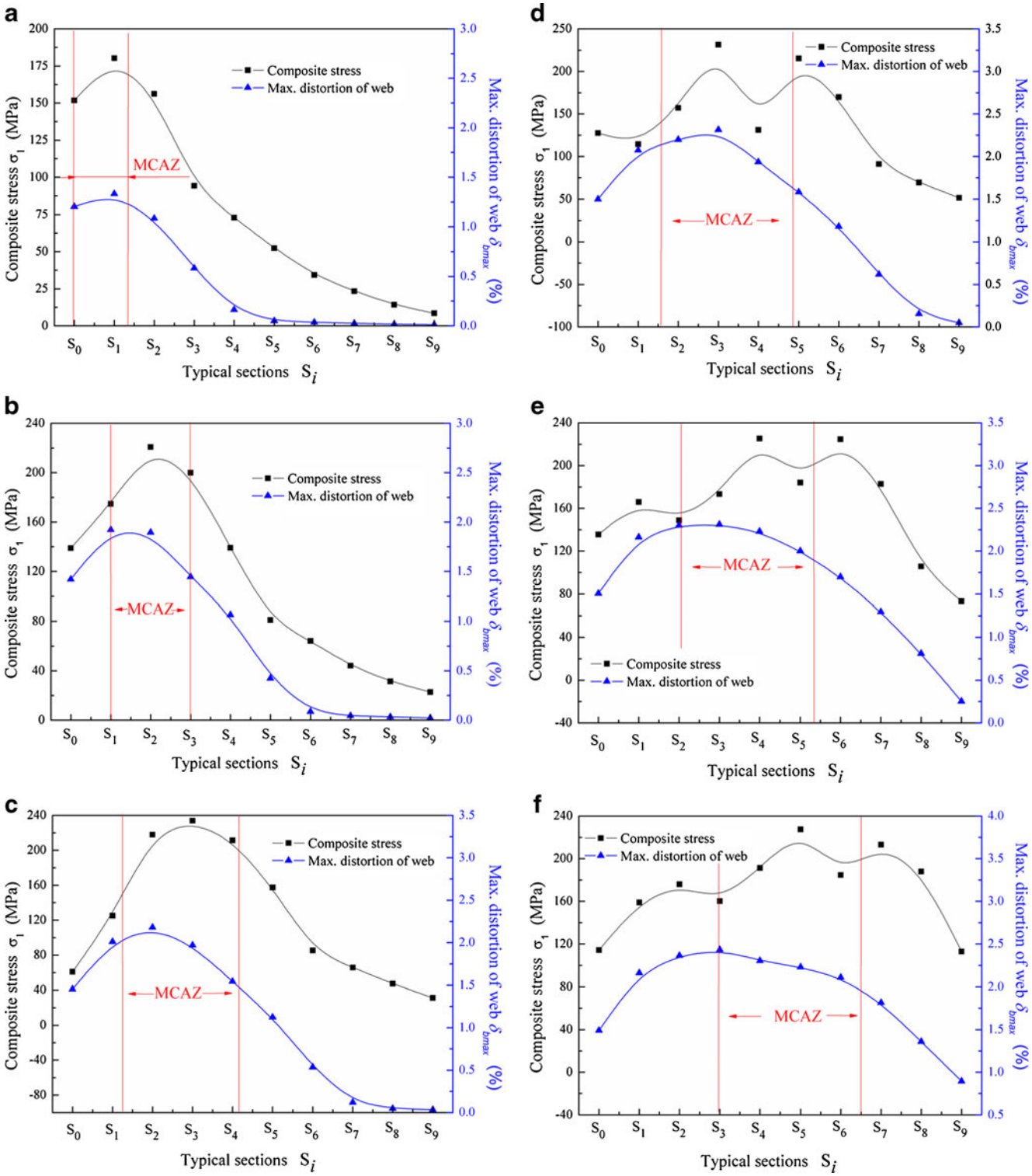

Fig. 13 The composite stress and the maximum web distortion during the bending stage: **a** bending angle, 10°; **b** bending angle, 20°; **c** bending angle, 30°; **d** bending angle, 40°; **e** bending angle, 50°; **f** bending angle, 60°; **g** bending angle, 70°; **h** bending angle, 80°; **i** bending angle, 90°; and **j** after mandrel retracting

influence on the stress distribution. Different cores number may lead to difference in stress distribution. Thus, according to the analysis above, the distribution of the cross-sectional distortion of TWRWT could be changed subsequently. To

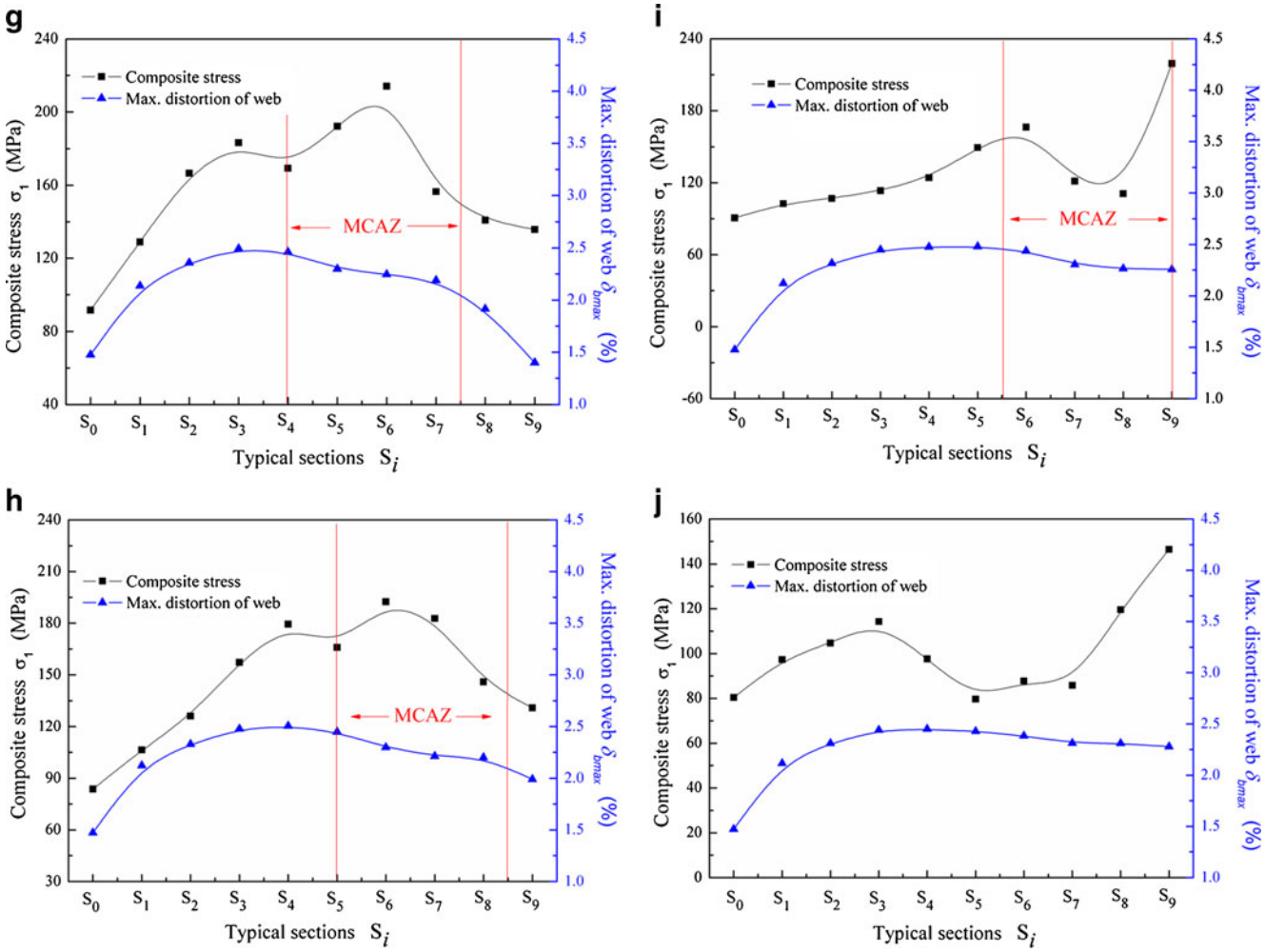

Fig. 13 (continued)

verify the above conclusion that δ_{h_i} have a close relation with σ_β while δ_{b_j} have a close relation with σ_1, the cross-sectional distortion and the corresponding stress components are obtained with different cores number.

Figure 14a shows the maximum distortion of the flange $\delta_{h_{\max}}$ and the circumferential stress σ_β with different cores number (2, 3, and 4, respectively). It can be seen that (1) the variation of σ_β as along with the values of $\delta_{h_{\max}}$ decrease when more cores are used; (2) the variation of σ_β as well as the values of $\delta_{h_{\max}}$ are much larger with two cores than those with three and four cores; (3) in the MCAZ S_6–S_9, there is little difference of σ_β among the three curves. The discrepancy in $\delta_{h_{\max}}$ among the three cases is little too. (4) Compared with three cores, four cores make little improvement on $\delta_{h_{\max}}$ and σ_β, so three cores are enough in practice. According to the analysis above, different cores number changes the distribution of σ_β, thus, $\delta_{h_{\max}}$ varies subsequently.

For completeness, comparisons between the maximum web distortion $\delta_{b_{\max}}$ and the composite stress σ_1 with different cores number are conducted (Fig. 14b). The obtained results confirm the relation between $\delta_{b_{\max}}$ and σ_1.

4.4 Discussion and guidelines

Mostly, the web distortion δ_{b_j} are much smaller than the flange distortion δ_{h_i} when flexile cores are used. Therefore, the web distortion δ_{b_j} are neglected in the below discussion. The results of Sections 4.1 and 4.2 indicate two ways to reduce the flange distortion δ_{h_i}. One effective way is to enlarge the area of MCAZ or CAZ since the two zones have less distortion. For example, a larger mandrel extension length [23] or more cores will be helpful since they can increase the area of MCAZ. At the same time, as shown in Fig. 15, larger clamp pressure F_c will also decrease the flange distortion due to the increase of CAZ. The other way to reduce the flange distortion is to smoothen the stress components. That's why decreasing the clearance between the mandrel die and the tube could bring positive results [19–21]. Additionally, decreasing the friction coefficient

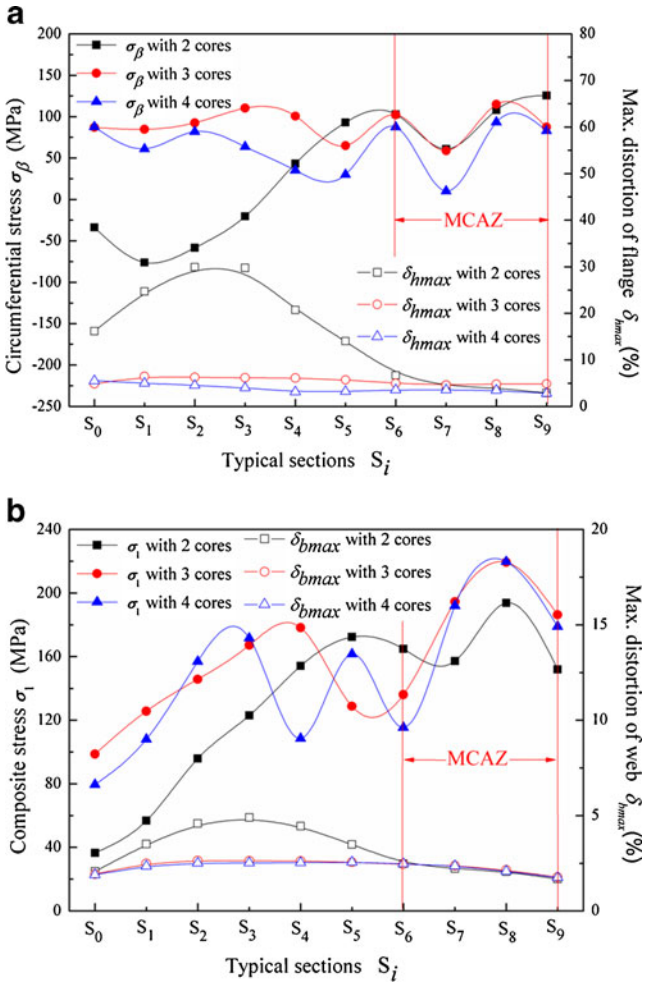

Fig. 14 The cross-sectional distortion and the corresponding stress components with different cores number: **a** the circumference stress and the maximum flange distortion and **b** the composite stress and the maximum web distortion

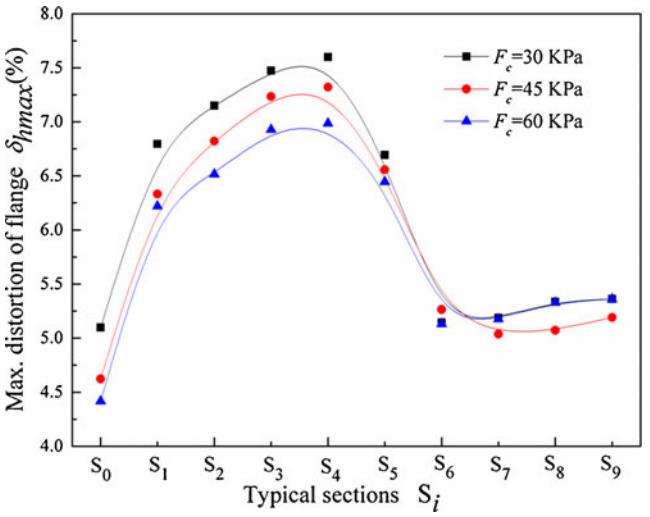

Fig. 15 Effect of clamp pressure on maximum distortion of flange

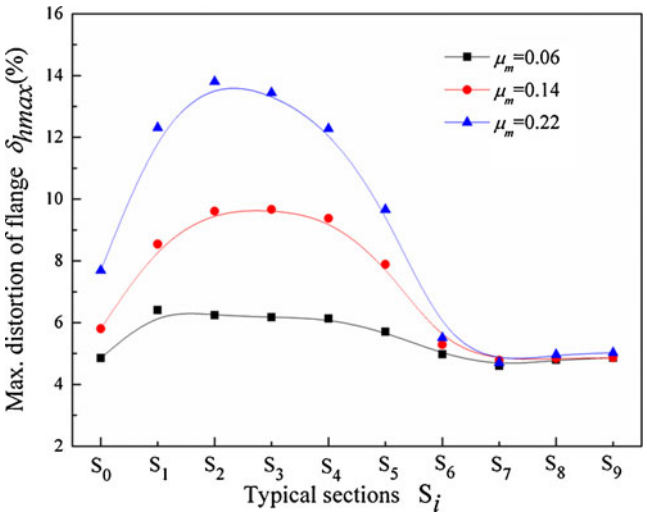

Fig. 16 Effect of friction coefficient between mandrel die and tube on maximum distortion of flange

between the mandrel die and tube μ_m could lower the flow resistance of tube bending [24]. As a result, the flange distortion δ_{h_i} decreases with the decrease of μ_m (shown in Fig. 16). Thus, the mandrel die should be well lubricated in practice.

5 Conclusions

1. The deformation zone of the tube can be divided into three sub-zones according to the loads and deformation, viz., the CAZ, the MZ, and the MCAZ.
2. The maximum flange distortion $\delta_{h_{\max}}$ locates at the symmetric line while the maximum web distortion $\delta_{b_{\max}}$ locates at the extrados ridge in each typical section. Flange distortion δ_{h_i} in the CAZ and the MCAZ are smaller than those in the MZ. At the same time, web distortion δ_{b_j} in the MCAZ and the MZ are larger than those in the CAZ.
3. The flange distortion has a close relation with the circumferential stress σ_β. The distribution and value of the maximum flange distortion $\delta_{h_{\max}}$ are determined by σ_β. At the same time, the web distortion is relevant to both the circumferential stress σ_β and the tangential stress σ_α. The distribution and value of the maximum web distortion $\delta_{b_{\max}}$ are determined by a comprehensive effect of the two stress components.
4. The relations between the cross-sectional distortion and the corresponding stress components are verified by FE models with different cores numbers. The obtained results confirm the relations between them. Moreover, some guidelines are introduced to help reduce the cross-sectional distortion in practice.

Acknowledgments The authors would like to thank National Natural Science Foundation of China (No. 50975235), Specialized Research Fund for the Doctoral Program of Higher Education (No. 20116102110012), and 111 Project (No. B08040) for the support to this research.

References

1. Li H, Yang H (2011) A study on multi-defect constrained bendability of thin-walled tube NC bending under different clearance. Chinese J Aeronaut 24:102–112. doi:10.1016/S1000-9361(11)60013-7
2. Vollertsen F, Sprenger A, Kraus J, Arnet H (1999) Extrusion, channel, and profile bending: a review. J Mater Process Technol 87:1–27. doi:10.1016/S0924-0136(98)00339-2
3. Yang H, Li H, Zhang ZY, Zhan M, Liu J, Li GJ (2012) Advances and trends on tube bending forming technologies. Chinese J Aeronaut 25:1–12. doi:10.1016/S1000-9361(11)60356-7
4. Paulsen F, Welo T (2001) Cross-sectional deformations of rectangular hollow sections in bending: part II—analytical models. Int J Mech Sci 43(1):131–152. doi:10.1016/S0020-7403(99)00107-1
5. Lucian L (2012) Effect of internal fluid pressure on quality of aluminum alloy tube in rotary draw bending. Int J Adv Manuf Technol. doi:10.1007/S00170-012-3992-8
6. Jiang ZQ, Zhan M, Yang H, Xu XD, Li GJ (2011) Deformation behavior of medium-strength TA18 high-pressure tubes during NC bending with different bending radii. Chinese J Aeronaut 24:657–664. doi:10.1016/S1000-9361(11)60077-0
7. Tang NC (2000) Plastic-deformation analysis in tube bending. Int J Press Vessel Pip 77(12):751–759. doi:10.1016/S0308-0161(00)00061-2
8. Liu YF, Daxin E (2011) Effects of cross-sectional ovalization on springback and strain distribution of circular tubes under bending. J Mater Eng Perform 20(9):1591–1599. doi:10.1007/s11665-010-9813-z
9. Goodarzi M, Kuboki T, Murata M (2007) Effect of die corner radius on the formability and dimensional accuracy of tube shear bending. Int J Adv Manuf Technol 35:66–74. doi:10.1007/s00170-006-0697-x
10. Miller JE, Kyriakides S, Corona E (2001) On bend-stretch forming of aluminum extruded tubes—II: analysis. Int J Mech Sci 43(5):1319–1338. doi:10.1016/S0020-7403(00)00040-0
11. Paulsen F, Welo T, Sovik OP (2001) A design method for rectangular hollow sections in bending. J Mater Process Technol 113(1–3):699–704. doi:10.1016/S0924-0136(01)00671-9
12. Welo T, Baringbing HA (2009) On the evaluation of dimensional accuracy in rotary stretch bending. Int J Mater Form (Suppl) 1:849–852. doi:10.1007/s12289-009-0642-2
13. Welo T, Wideroe F (2010) Precision bending of high-quality components for volume applications. Trans Nonferrous Met Soc China 20:2100–2110. doi:10.1016/S1003-6326(09)60425-8
14. Tian S, Liu YL, Zhao GY, Yang H (2010) Experimental research on strain distribution characteristics of thin-walled rectangular tube in rotary-draw bending. Adv Mater Res 139–141:502–505. doi:10.4028/www.scientific.net/AMR.139-141.502
15. Liu KX, Liu YL, Yang H, Zhao GY (2011) Experimental study on cross-section distortion of thin-walled rectangular 3A21 aluminium alloy tube by rotary draw bending. Int J Mater Prod Techno 42:110–120. doi:10.1504/IJMPT.2011.044888
16. Li H, Yang H, Liu K (2012) Towards an integrated robust and loop tooling design for tube bending. Int J Adv Manuf Technol. doi:10.1007/S00170-012-4258-1
17. Mentella A, Strano M, Gemignani R (2008) A new method for feasibility study and determination of the loading curves in the rotary draw-bending process. Int J Mater Form (Suppl) 1:165–168. doi:10.1007/s12289-008-0017-0
18. Tang D, Li DY, Yin ZW, Peng YH (2009) Roles of surface booster system on bending of thin-walled copper tube. J Mater Eng Perform 18:369–377. doi:10.1007/s11665-008-9300-y
19. Zhao GY, Liu YL, Yang H (2010) Effect of clearace on wrinkling of thin-walled rectangular tube in rotary draw bending process. Int J Adv Manuf Technol 50:85–92. doi:10.1007/s00170-009-2508-7
20. Liu YL, Lu CH, Zhao GY, Yang H (2008) Effect of clearance on cross section distortion of thin-walled rectangular tube in rotary draw bending process. China Mech Eng 19(16):1972–1975 (in Chinese)
21. Zhao GY, Liu YL, Yang H, Lu CH (2010) Cross-sectional distortion behaviors of thin-walled rectangular tube in rotary-draw bending process. Trans Nonferrous Met Soc China 20(3):484–489. doi:10.1016/S1003-6326(09)60166-7
22. Zhao GY (2010) Study on wrinkling behaviors and limit during NC rotary-draw bending process of thin-walled rectangular tube. Ph.D. thesis, Northwestern polytechnical university, China [in Chinese]
23. Gu RJ, Yang H, Zhan M, Li H, Wang GX (2005) Effect of mandrel on cross section quality of thin-walled tube numerical controlled bending. Trans Nonferrous Met Soc China 15(6):1264–1274
24. Yang H, Gu RJ, Zhan M, Li H (2006) Effect of frictions on cross section quality of thin-walled tube NC bending. Trans Nonferrous Met Soc China 16:878–886. doi:10.1016/S1003-6326(06)60344-0